Nonlinear effects for coda-type elastic waves in stressed granular media

V. Tournat*
LAUM, CNRS, Université du Maine, Avenue O. Messiaen, 72085 Le Mans, France

V. E. Gusev
Laboratoire de Physique de l'État Condensé, UMR-CNRS 6087, Université du Maine, Avenue O. Messiaen, 72085 Le Mans, France
(Received 22 May 2008; revised manuscript received 20 April 2009; published 17 July 2009)

Experimental results and their interpretations are presented on the nonlinear acoustic effects of multiple scattered elastic waves in unconsolidated granular media. Short wave packets with a central frequency higher than the so-called cutoff frequency of the medium are emitted at one side of the statically stressed slab of glass beads, and received at the other side after multiple-scattering and nonlinear elastic effects. Typical signals are strongly distorted compared to their initially radiated shape both due to nonlinearity and scattering. It is shown that acoustic waves with a deformation amplitude much lower than the mean static deformation of the contacts in the medium can modify the elastic properties of the medium. This addresses the problem of acoustic wave action on granular matter during and after acoustic excitation, which is necessary to understand in the nondestructive testing of the elastic properties of granular media by acoustic methods. Coda signal analysis is shown to be a powerful time-resolved tool in monitoring slight modifications in the elastic response of an unconsolidated granular structure.

DOI: 10.1103/PhysRevE.80.011306 PACS number(s): 45.70.−n, 46.40.Cd, 43.25.+y

I. INTRODUCTION

Unconsolidated granular materials are known to exhibit a high complexity in their macroscopic behaviors. This gives rise to numerous fundamental and applied processes that are currently intensively studied, such as avalanches, dune formation, compaction, etc. [1–4]. Most of the studied physical processes concerning the unconsolidated granular matter are obviously related to the possibility for the grains to move relative to each other, from microscopic (much smaller than a grain diameter) to macroscopic (much larger than a grain diameter) rearrangements. While large movements of grains have been observed and modeled for the processes where the granular material behavior may be fluidlike (even complex and not classical), such as avalanches, microscopic relative movements are less intuitive and less studied. They are, however, the only possible relative movements in solidlike granular media where a static stress is applied and the grains are confined in a given volume.

In this context, the acoustic waves, known to be highly sensitive to the contact stresses [5–8], can be useful for monitoring of these small relative movements [9], which are impossible to detect by other existing methods. They could even be useful for the generation of these small movements. Among the several existing methods for the grain movement or contact stress monitoring (carbon paper experiment, photoelasticity, image processing from charge-coupled device camera, x-ray tomography, or photoimaging in isoindex configuration [2,4,10,11]), the acoustic methods are, to the best of our knowledge, the only ones sensitive to the contact stresses inside the volume of a three-dimensional (3D) nontransparent medium. One of the main advantages of acoustic methods is also the temporal resolution of the measurement, which could decrease down to the wave period (one millisecond at one kHz), and is particularly interesting in transient processes such as avalanches for instance. However, there is currently a lack of understanding of the acoustic transport properties through granular media, which makes these methods mostly qualitative.

Several previous studies [7,9,12,13] have shown the following qualitative features for the acoustic wave propagation through stressed and noncohesive granular media. The propagation of a low amplitude (with a strain much lower than the average static strain of the contacts) and low-frequency (LF) (with a wavelength much larger than the grain diameter) wave can be linear, and is mostly governed by the averaged properties of the medium (average density, average static stress, coordination number) [14,15]. The propagation of a high amplitude (with a strain lower than the average static strain of the contacts but which can be comparable) and low-frequency wave is nonlinear, and governed partly by the so-called weak contacts (with a static strain lower than the average one) [7,16–18]. This is a consequence of the fact that individual stress-strain relationships for each contact have higher values of nonlinear parameters when the prestress is smaller. For acoustic waves with wavelengths comparable to the bead diameter, however, these simple features are not straightforward, and the transport property determination remains a fundamental problem. A linear diffusion approach has been recently applied to the analysis of coda-type signals in confined granular media [8]. This is one of the first attempts to understand the transport properties of short-wavelength elastic waves in such media at the laboratory scale, and to extract parameters such as a characteristic time of absorption τ_a and a diffusivity D. This approach is based on previous works in elastic wave diffusion carried out for slightly different media (solid rods in water [19], chaotic cavities [20], or glass bead in water [21] for instance) and on a different scale [22,23].

*vincent.tournat@univ-lemans.fr

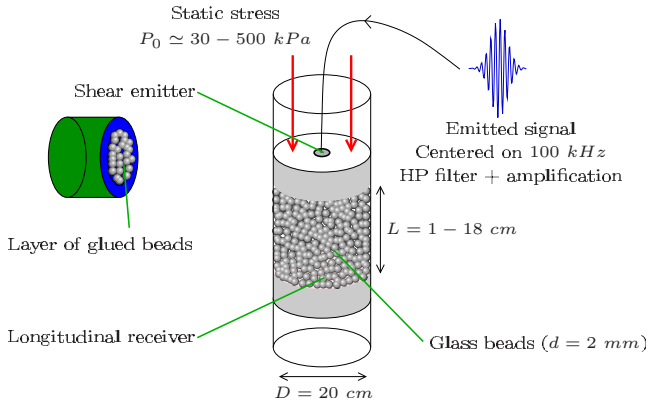

FIG. 1. (Color online) Schematics of the experimental configuration.

In this paper, we report experimental results of nonlinear acoustic wave interactions in granular matter, with initially radiated wavelengths close to the bead diameter. In some well-chosen experimental configurations, it is possible to observe coda-type signals, together with a nonlinear signal of low frequency, which is identified here as a self-demodulated signal. The main aims of this paper are to report selected experimental observations that contribute to understand (i) what is the nature of short-wavelength elastic wave transport in granular media, (ii) from which strain excitation amplitude relative to the average static strain do the waves begin to modify the granular packing elasticity, and (iii) why coda wave shapes are extremely sensitive to the acoustic excitation amplitude and to the external conditions applied on the granular packing?

Among the presented experimental observations, features that have not been reported in the literature should contribute to the understanding of the elastic wave interactions with granular matter. In the first part we present the experimental configuration and the results of the investigations on the nature of the transmitted signals. In the second part, we analyze in detail the amplitude dependence of the multiple scattered signals using a sequence of different excitation amplitudes that allows observation of elastic wave-granular matter reversible and irreversible interactions. In the last part, the main results are summarized and interpreted. The applications of some of the presented effects to the characterization of granular media are finally discussed.

II. SETUP AND PRELIMINARY EXPERIMENTS

A. Experimental setup

In Fig. 1, a schematic representation of the experimental setup is shown. A wave packet made of a sine wave at 100 kHz modulated in amplitude by a Gaussian function is high-pass filtered over 40 kHz (in order to avoid any direct low-frequency excitation), and is amplified and launched in the medium with a shear piezotransducer. Due to multiple scattering and mode conversions (including dilatancy [7]), the acoustic energy is rapidly distributed between longitudinal and shear vibrations in the medium. The use of a shear emitter has the advantage of avoiding the direct excitation of a pressure wave in the air saturating the beads. It consequently excites preferentially the elastic waves inside the granular solid skeleton (the beads and their contacts). In the following results, two types of Gaussian function widths for the initially launched wave packets have been used, and two types of surface treatment for the shear transducer (the first type is the raw transducer membrane with asperities estimated to be of characteristic scale $\sim 50\ \mu$m and the second type is a transducer with a glued single layer of 2-mm-diameter glass beads, the same beads as in the medium itself). The container diameter is $D=20$ cm, and the distance emitter-receiver can be changed between 1 and 18 cm. The applied static uniaxial stress is measured with a force sensor at one end of the container and ranges from 30 to 500 kPa. A longitudinal piezoelectric receiver is placed at the bottom of the container. This transducer has been chosen because of its high sensitivity over a wide-frequency band, allowing for a large range in the acoustic amplitude measurements. In all the experiments presented in the following, the estimated average contact strain ε_0 (with a value $3-7\times10^{-4}$ for a 200 kPa applied stress) is always larger than the maximum acoustic strain $\varepsilon_{max} \simeq 10^{-5}$.

This setup allows modification of the emitted acoustic frequency and amplitude, the applied static stress, and the propagation distance. But importantly, it is better for a quantitative insight in the wave propagation phenomena to modify parameters of the setup that change the smallest number of medium (or wave) parameters. The convenient parameter to be modified is the wave excitation amplitude, which can be accurately measured, and is reproducible. In the following, signal dependences on different parameters of the experiment are described in order to understand the physical nature of the detected signals and the main processes involved.

B. Dependence of the coda-type signals on the excitation amplitude

Temporal signals presented in Fig. 2 are typical experimental signals that can be observed when the initial acoustic wavelength is of the order or less than the bead size and for a static stress larger than ~ 100 kPa. For an estimation of the wavelength, one can use the elastic parameters of glass and the stress-strain relationship of an average loaded contact in an effective-medium theory. However, it is important to keep in mind that this definition neglects wave velocity dispersion, which can be important when the spatial scale of the beads is comparable with the wavelength. As an estimation, the wave velocity in a disordered three-dimensional packing of 2 mm glass beads with an applied static stress of 200 kPa is $c_0=300\pm40$ m/s, which gives a wavelength of 3 ± 0.4 mm at 100 kHz. This means that, for a wave packet centered on 100 kHz, submitted to a 200 kPa static stress, the wavelength is of the order of the bead diameter, and consequently, strong scattering occurs.

The typical experimental signals received in this case are strongly distorted due to multiple scattering, and last from 10 to 100 times longer than the emitted signal of duration $\sim 100\ \mu$s (see Fig. 2). Note that the chosen configuration

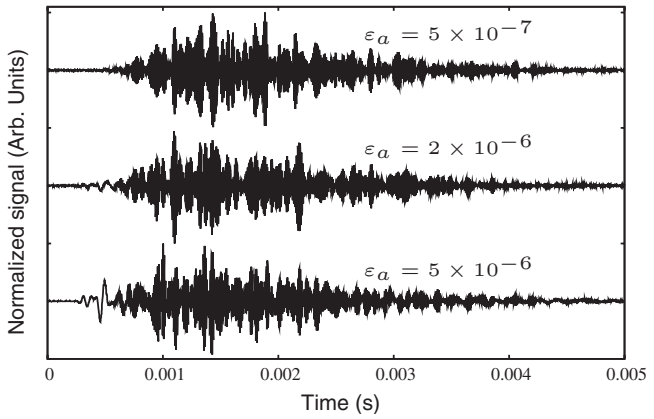

FIG. 2. Experimental temporal signals (normalized) that are typically received for different excitation amplitudes in the same bead packing. The applied static stress is $\sigma_0 = 300 \pm 5$ kPa and the emitter-receiver distance is $D = 10.5 \pm 0.1$ cm. Peak-to-peak amplitudes of the non-normalized signals are roughly proportional to the excitation amplitudes ε_a.

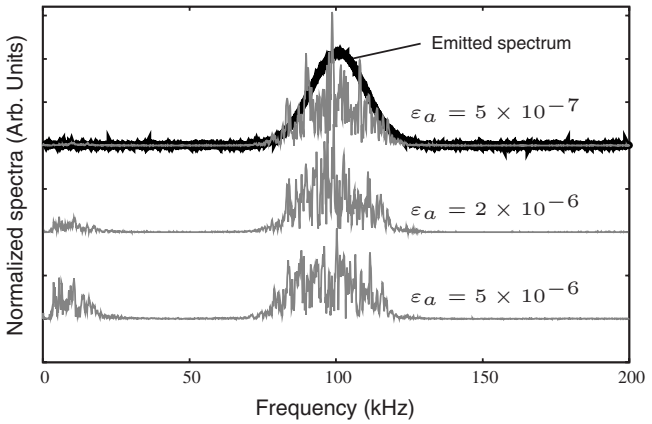

FIG. 3. Experimental spectra corresponding to temporal signals of Fig. 2. The spectrum of the emitted signal with a 22% full width at half maximum (FWHM) is superimposed on the top curve.

with a shear emitter and a longitudinal receiver is particularly suitable for such observation of multiple scattered signals as the initially purely shear wave has to be scattered with a conversion from shear to longitudinal polarization in order to be detected. These types of signals have been observed in similar conditions in glass bead assemblages [12], and are widely observed in multiple-scattering experiments and in seismics [22]. They are consequently denoted here as coda signals. We found, however, another feature in this case, not mentioned previously in the literature: for different excitation amplitudes, the normalized signals in Fig. 2 (obtained for the same bead packing) are different. The relative amplitude and shape dependence are the signature of a nonlinear process. One obvious difference between the traces is the emergence, for an increasing excitation amplitude, of a signal at earlier times, relatively lower in frequency than the 100 kHz coda-type signal. We verified in several other experiments [7,13] that this LF signal is the self-demodulated contribution associated with the rectification (demodulation) of the initial high-frequency (HF) wave packet. Its nonlinear nature is evidenced by its nonlinear amplitude dependence on the excitation amplitude. This is an important difference compared to results [8,12], where the very same types of signals were observed (for instance for $\varepsilon_a = 5 \times 10^{-6}$ in Fig. 2). In [12], the LF contribution is identified as the linear coherent part of the propagated initial pulse, and the HF contribution is interpreted as the multiply scattered signal part. A possible explanation for such a different observation (in the amplitude dynamics behavior and physical nature of the LF signal) is the difference in the spectral width of the emitted signal. In Ref. [12], the signal spectrum width is relatively wide, which may allow for the direct radiation of the linear coherent LF component in the medium. Then, the observation may be interpreted as a strong frequency dependent transmission in the medium (due to absorption and scattering), which is able to modify importantly the transport character of different frequencies (propagative as in an effective medium, multiply scattered, diffusive, etc.).

Here, as the emitted spectrum is sharper than in Ref. [12], the direct radiation of the LF signal is negligible (and in any case is avoided by the high-pass filter in the setup). This LF signal is generated in the medium itself by a nonlinear wave process of frequency mixing [7], widely described in the literature [24–28]. This can be seen in Fig. 3, where the relative amplitudes of the LF and the HF contributions are modified by increasing the excitation amplitude. However, note that this process is inefficient for shear waves in homogeneous solids for symmetry reasons but can be observed here due to the mode conversion from shear to longitudinal wave occurring due to inhomogeneities and due to the strong nonlinear dilatancy [7].

C. Dependence on emitter-receiver distance

In Fig. 4, the received temporal signals are presented for three source-receiver distances, with the same applied static

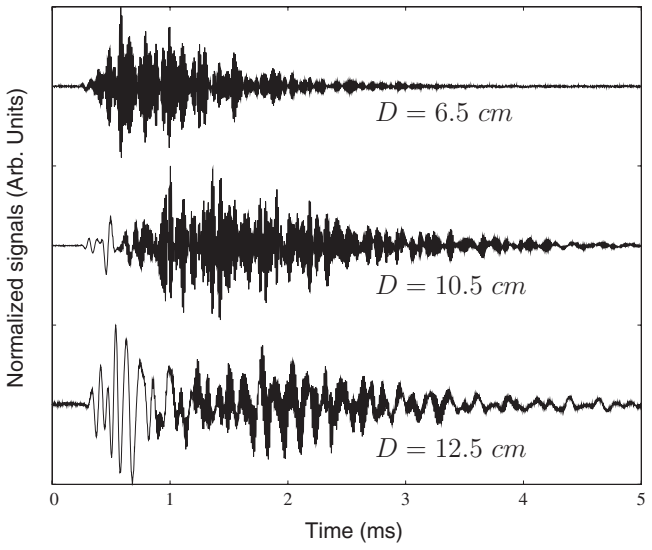

FIG. 4. Signals received after propagation through different thicknesses of granular medium, for identical static pressure of 300 kPa and excitation amplitude $\varepsilon_a = 5 \times 10^{-6}$.

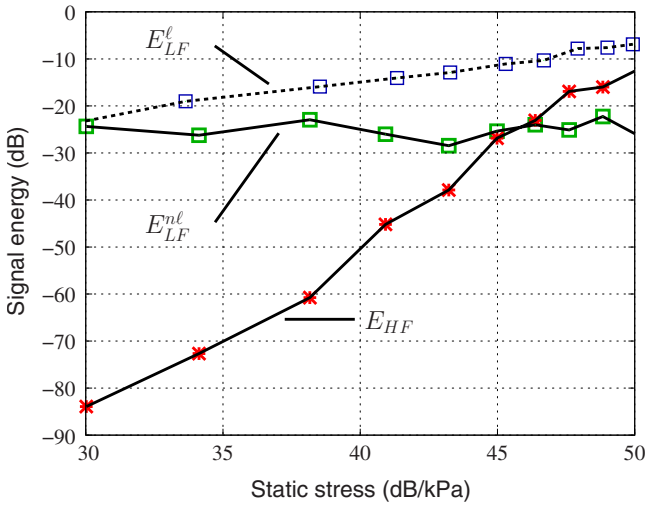

FIG. 5. (Color online) Signal energy variation as a function of the applied static pressure. The HF (E_{HF}) and LF ($E^{n\ell}_{\mathrm{LF}}$) contributions are separated by filtering. The energy of a reference LF (E^{ℓ}_{LF}) linear signal is also plotted for comparison.

stress of 300 kPa (measured with a precision of ~3%, which is not sufficient to perform precise quantitative measurements). An important qualitative feature observed on these normalized (by their maximum) traces is the relative increase in the LF contribution compared to the HF one with distance. This feature is usually observed for the nonlinear self-demodulation process [25], where, over a sufficient distance, only the LF contribution is detectable due to the difference in attenuation of the HF and the LF waves. In this experiment, the LF signal energy is measured to be roughly constant with distance while the received HF signal energy is decreasing drastically. The former is a result of the competition between nonlinear acoustic effects, which pump low frequencies through frequency-down-conversion processes, and linear attenuation.

D. Dependence on the applied static stress

In Fig. 5, the total energy of different signals is plotted as a function of the applied static stress for a propagation distance $D=12.5\pm0.1$ cm and an excitation amplitude $\varepsilon_a \simeq \varepsilon_{max}/50$, where $\varepsilon_{max}\simeq 10^{-5}$. Three signal energies are defined here: the energy of the HF contribution E_{HF}, the energy of the LF contribution $E^{n\ell}_{\mathrm{LF}}$, and the energy of a directly radiated LF signal E^{ℓ}_{LF} (in this case, a LF pulse with the same frequency content as the nonlinearly demodulated pulse is directly excited by the emitter and received after linear propagation). First, comparing the evolution of the received energies E_{HF} and E^{ℓ}_{LF} as a function of the applied static stress, an important slope difference is clearly visible: E^{ℓ}_{LF} dependence is less than to a power 1 of the stress and E_{HF} dependence is close to a power 4 of the stress. In order to explain this difference in the evolution of the transmitted energy as a function of the applied static stress, one should recall that two dominant processes of sound attenuation may play a role: the scattering and the absorption due to linear processes. Considering that the scattering of the HF wave at 100 kHz is much more important than for the LF wave at 10 kHz, the observed difference may be attributed to the strong stress dependent scattering. This is consistent with the simple idea that, by increasing the static stress, contacts are created and then add new paths (or strengthen existing paths) of acoustic energy transmission. Moreover, waves following force chains with a given stress may change from an evanescent character to a propagative one with increasing stress because the cutoff frequency (sometimes called the Einstein frequency) is increased [29–31]. It is then possible to ask, given the dramatic influence of the static stress on E_{HF}, if this scattering could depend also on the acoustic amplitude of excitation. Is the acoustic wave able to dynamically switch propagation paths or force chains? The aim of the next section is to analyze this opportunity and its possible manifestations.

The competition between nonlinear effects and attenuation is also visible in Fig. 5 when comparing the variations in E^{ℓ}_{LF} and $E^{n\ell}_{\mathrm{LF}}$. For signals having the same low frequency and propagating through the same medium but generated either directly by a transducer or by nonlinear acoustic effects during wave transport, their received energies increase differently as a function of the applied static stress. It can be assumed that the linear attenuation varies in the same way for both signals. In contrary, the nonlinearity of the medium and the HF attenuation, both playing a role in the generation of the LF signal [25], may be strongly affected. The latter modifications should only affect the nonlinearly generated signal. $E^{n\ell}_{\mathrm{LF}}$ variation as a function of the applied static stress is almost negligible while E^{ℓ}_{LF} is increasing. It means that the efficiency of the nonlinear wave interactions leading to the self-demodulated signal is decreasing with increasing static stress. Two main processes can lead to a diminishing of the nonlinear wave interaction efficiency: the HF attenuation increases (the amplitude of the nonlinear wave sources diminishes) and the intrinsic nonlinearity of the medium decreases. As the HF attenuation (probed by the variation in E_{HF}) is strongly diminishing with increasing static stress, it means that the nonlinearity of the medium is decreasing with increasing static stress. This is consistent with estimates based on the Hertzian contact nonlinearity and other experimental observations [7,13].

III. ANALYSIS OF AMPLITUDE DEPENDENT CODAS

Fast dynamic modifications of the medium submitted to an acoustic wave, as well as slow-dynamic modifications or permanent modifications of the medium are now investigated. The experimental configuration is slightly different from the one in the previous section. Some glass beads have been glued to the shear emitting transducer surface, in order to couple better to the medium and to improve the signal-to-noise ratio.

The analysis of the obtained spectra indicates that it is impossible to detect neither the second nor the third harmonic component, certainly due to the strong observed attenuation above 100 kHz. However, the self-demodulated wave is quite easily generated and detected because of its lower attenuation. In the following, the HF coda contribution

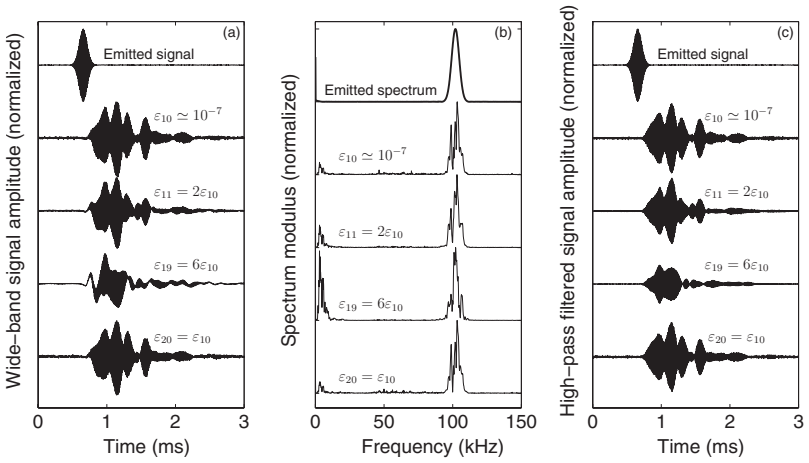

FIG. 6. Typical temporal signals (normalized by the excitation amplitude) that are received at a distance of 6 cm from the emitter for different excitation amplitudes. The emitted signal is a Gaussian wave packet centered on 100 kHz with a FWHM of 6% in frequency. (a) Row temporal signals. (b) Amplitude spectra of the row signals. (c) High-pass filtered signals.

and this LF self-demodulated contribution are separated by postprocessing filtering in order to analyze in details the different amplitude-dependent processes.

In Fig. 6(a), typical temporal signals that are received by a sensitive wide-band longitudinal transducer (with a sensitive surface of 4.5 cm in diameter) are presented. The experimental excitation amplitude sequence (EAS) elaborated in order to analyze the amplitude-dependent effects of acoustic wave transport is presented in Fig. 7(d). It contains 59 successive excitation amplitudes. The ten first amplitudes, as well as the last ten amplitudes, are identical and relatively low (the acoustic strain is $\varepsilon_a = \varepsilon_{1-10} \simeq 10^{-7}$). The odd numbered amplitudes 11–49 of this sequence are gradually increasing up to a maximum amplitude of $\varepsilon_a \simeq 10^{-5}$, while the even numbered amplitudes 10–50 are equal to the minimum probe amplitude $\varepsilon_a \simeq 10^{-7}$. This allows comparison of the response of the medium for different excitation amplitudes, but also, to visualize the medium modifications after being excited by a strong wave by using the weak probe wave. The experiment time for the acquisition of one signal of this EAS is close to 30 s. In Fig. 6, signals are numbered according to their excitation amplitude in the EAS, the first signal of the EAS being denoted by s_1. The excitation signal is a sine wave modulated in amplitude with a Gaussian function of 6% full width at half maximum (FWHM) in the frequency domain, which, at the central frequency $f_0 = 100$ kHz gives a ~ 0.2 ms duration pulse at half the maximum. This duration is roughly the time necessary for the wave to travel from the emitter to the receiver for the 6 cm distance.

In Fig. 6(a), received signals over the full available frequency band (from 1 to 300 kHz) are presented for several excitation amplitudes of the EAS: ε_{10}, ε_{11}, ε_{19}, ε_{20}. The signal structure is quite complicated and shows several packets typically four to five, having a shape close to the emitted signal. It is important to note here that the time dependent intensity of these signals is much different from a diffusive type envelope, even if the average wavelength is of the order of the bead radius. Another important feature is the emergence, at a sufficiently high excitation amplitude of a relatively low-frequency signal [see for instance signal s_{19} corresponding to the amplitude ε_{19} in Fig. 6(a) and the corresponding amplitude spectrum in Fig. 6(b)]. Due to its amplitude-dependent character (this signal is not visible for lower excitation amplitudes), this LF signal is nonlinear, and has been identified in the previous section as being the self-demodulated contribution [7,13].

In the following, we analyze the high-frequency part of the signals, and for quantitative comparison, the raw signals are high-pass filtered [Fig. 6(b)]. These coda-type signals have comparable time durations to those of Fig. 2 but their envelope characteristic frequency is lower. This is a consequence of the narrower Gaussian spectrum of excitation compared to the previous section. However, despite the dif-

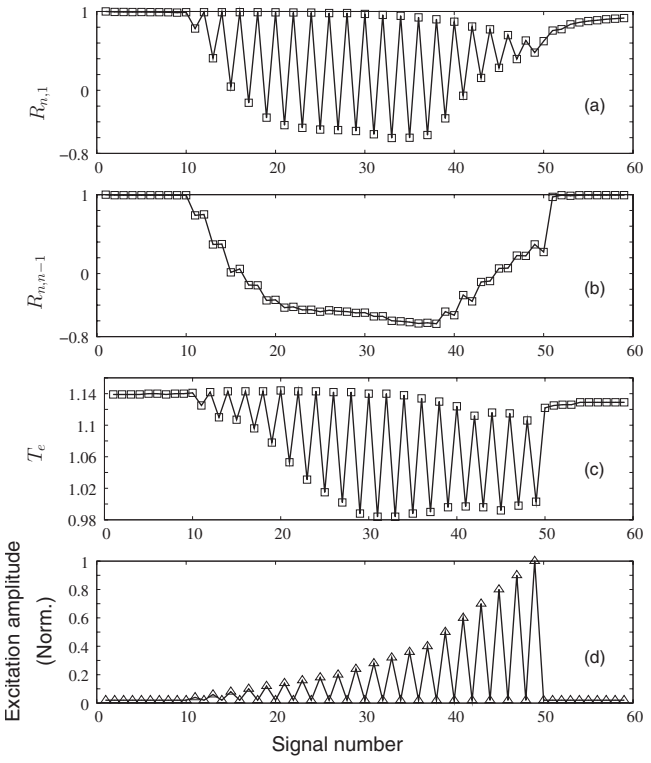

FIG. 7. (a) Resemblance parameter $R_{n,1}$ between the signal number n and the signal number 1 of the excitation amplitude sequence (EAS) (d). (b) Resemblance parameter $R_{n,n-1}$ between the signal number n and the signal number $n-1$ of the EAS (d). (c) Arrival time T_e of half the signal energy as a function of the signal number in the EAS (d). (d) Excitation amplitude sequence (EAS) used in the experiment.

ference in coda shape, the characteristics of wave transport are similar.

A. Dependence of the signal shape on excitation amplitude

The most important characteristics of the signal evolution with excitation amplitude is the fact that their temporal shape is strongly modified, even for very moderate changes in the excitation amplitude. This can be seen by comparing the shapes s_{10} and s_{11} in Fig. 6(c). Of course, by increasing further the excitation amplitude, the distortion is further increased (signal s_{19}). When the excitation amplitude is decreased down to the lowest amplitude of the EAS, i.e., to the probe amplitude ε_1, the shape modification of s_{20} compared to s_1 is barely noticeable.

In order to monitor quantitatively the modifications of the signal shapes due to amplitude-dependent effects, we make use of the following parameter $R_{m,n}$ defined from the intercorrelation function $C_{n,m}(\tau)=\int_0^T s_n(t)s_m(t-\tau)dt$, where T is the observation window duration, by

$$R_{n,m}=\frac{C_{n,m}(0)}{\sqrt{C_{n,n}(0)C_{m,m}(0)}}. \tag{1}$$

The energy of signal s_n (s_m) is proportional to $C_{nn}(0)$ $[C_{mm}(0)]$. The normalization by $\sqrt{C_{nn}(0)C_{mm}(0)}$ makes consequently the parameter $R_{n,m}$ independent of the actual energies of s_n and s_m, which is important in our case where signals with different amplitudes are compared. The parameter is only dependent on the relative shapes of the signals and can be seen as the level of resemblance of two signals, equal to one if the two signals are exactly the same and progressively diminishing when the signals differ.

In Fig. 7(a), the parameter $R_{n,1}$ is plotted for each signal s_1 to s_{59} of the EAS. It is clearly visible that the parameter $R_{11,1}$ goes under a value of 0.9 while the signals s_2 to s_{10} exhibit a very accurate correlation with $s_1(R_{2-10,1}\simeq 1)$. When the amplitude is increased further, the parameter $R_{n,1}$ decreases drastically to zero or less, which shows that a strong-field modification occurred (the negative values of the parameter $R_{m,n}$ do not have a particular meaning, except when the value reaches -1, which means that the signal phases are inverted). Concerning the even signals generated with a low excitation amplitude, their resemblance parameter remains practically equals to one up to the 30th signal of the EAS. This means that no modification of the granular medium elasticity is detectable by this acoustic probing. However, when higher acoustic amplitudes are generated in the medium, the level of resemblance of the probe wave with the first signals of the EAS begins to fall down progressively until the typical value of 0.6 after the maximum excitation strain ε_{49}. The acoustical properties of the medium have been modified by the strong wave action.

When, at the end of the EAS, only the probe amplitude is generated (signals s_{50} to s_{59}), the parameter $R_{n,1}$ tends to one with time; the acoustic properties of the medium are progressively recovered in a slow healing process. The parameter $R_{n,n-1}$ in Fig. 7(b) shows the level of resemblance of two successive signals. It is interesting to see that, in this healing process, two successive signals are practically identical, which makes this process slowly cumulative. This effect can be seen as a slow-dynamic effect observed for elastic waves in other materials too, such as sandstones and cracked solids [32,33]: the strong wave action modifies the acoustic properties of the medium, which are slowly recovered after some time, long compared to the wave period. The probing of this slow process is sometimes a powerful indication of damage (associated with the presence of internal contacts) in materials [34].

The last parameter plotted in Fig. 7(c) is the characteristic time T_e corresponding to the arrival time of half the total energy of the signal. It exhibits a quite clear amplitude dependence and has the same qualitative behavior as the parameter $R_{n,1}$. Until the 30th amplitude of the EAS $(\varepsilon_{33}\simeq 0.3\times 10^{-5})$, the characteristic time T_e of the probe wave (even numbered signals) remains unchanged while the signals $s_{11}-s_{31}$ exhibit a diminishing characteristic time T_e. It means that either the wave packet is propagating faster (nonlinear hardening of the medium) or the signal energy is preferentially attenuated at later times of the coda. Due to the strong nonlinear wave attenuation observed in the temporal signals of Fig. 6(c), the second process is more adequate to explain the T_e dependence on amplitude. This is visible in Fig. 6(c) when comparing signals s_{10} and s_{11} or s_{10} and s_{19}. No shift in time is detectable while the last part of the signals is strongly attenuated relatively to their first part. Possible interpretations of the above presented experimental observations are now given.

Qualitatively the influence of the nonlinear attenuation on the shape of the coda-type acoustic signal could be understood from the analysis of the nonlinear attenuation of the individual wave packets contributing to coda. Let us assume for simplicity that a particular wave packet is propagating with the same and constant group velocity $v_g=v_g(\omega)$. Distributed acoustic attenuation in the bulk of the medium leads to the dependence of the signals not just on the accompanying time $\tau=t-x/v_g$ prescribing the shape of a wave packet but also, additionally, slowly on time $s=s(t,\tau)$. Here x denotes the coordinate along the packet propagation path, which could be different for different packets. The group velocity $v_g(\omega)$ can be also different for different packets. In the following analysis we are not interested in the evolution of the wave-packet shape with time (or, equivalently, with propagation distance) but rather in the evolution of its amplitude. Neglecting the linear processes of wave-packet broadening due to dispersion of group velocity, the equation for the packet amplitude $s_A\equiv s(t=x/v_g)$ evolution can be written as

$$\partial s/\partial t+\omega_{at}(s)s=0. \tag{2}$$

Here $\omega_{at}(s)$ is the characteristic attenuation frequency (inverse of the attenuation time) at the central frequency of the wave packet, which depends in general on the wave-packet amplitude s. The general solution of this equation in the implicit form is

$$\int_{s(t)}^{s(0)}\frac{ds'}{\omega_{at}(s')s'}=t, \tag{3}$$

where $s(0)$ is the amplitude of the wave packet emitted at time $t=0$. Separating attenuation processes into amplitude-

independent (linear) and amplitude-dependent (nonlinear) processes $\omega_{at}=\omega_{LN}+\omega_{NL}(s)[\omega_{NL}(s)\geq 0]$, implicit solution (3) can be presented as

$$\frac{s(t)}{s(0)}=\exp(-\omega_{LN}t)\exp\left(-\int_{s(t)}^{s(0)}\frac{\omega_{NL}(s')/\omega_{LN}}{1+\omega_{NL}(s')/\omega_{LN}}\frac{ds'}{s'}\right). \tag{4}$$

The first exponential in Eq. (4) describes linear attenuation of the signal while the second exponential describes the influence of an additional nonlinear attenuation. Similar to the linear attenuation, bulk nonlinear attenuation exhibits accumulating influence on the wave packet. The longer the propagation time of a wave packet (or, equivalently, the larger its arrival time at the detector) and the smaller the $s(t)$, the larger is the integral in Eq. (4) and the stronger is the fall in signal amplitude relative to its magnitude in the absence of nonlinear absorption. Thus nonlinear absorption leads to preferential diminishing in amplitude of the tail of a coda-type signal, that is, to an apparent shortening of a coda-type signal in duration (localization of a coda-type signal in time). This effect can be also explained in different terms as follows. In case of a nonlinear attenuation, an increase in a signal amplitude leads to acceleration of the attenuation processes, a wave packet loses its energy faster in time. As a result of this at sufficiently long propagation times, the increase in attenuation nearly completely compensates the increase in initial signal amplitude. Thus increase in signal amplitude leads to preferential increase in amplitude of the leading part of the coda-type signal and corresponding shortening of the coda signal duration. The above presented model could provide a qualitative insight for the possible reasons of shortening in duration of coda signals s_{11} and s_{19} in comparison with s_{10} in Fig. 6(c).

For the model of linear dependence of attenuation on the wave amplitude $\omega_{NL}=\omega'_{NL}s$, which could be a good first (low but finite amplitude) approximation for most of the models of nonlinear absorption (in particular, for hysteretic absorption in stick-slip motion of Hertz-Mindlin contacts between the beads [35,36]) the solution of Eq. (3) can be presented in explicit form

$$\frac{s(t)}{s(0)}=\frac{\exp(-\omega_{LN}t)}{1+[\omega'_{NL}s(0)/\omega_{LN}][1-\exp(-\omega_{LN}t)]}, \tag{5}$$

confirming the predictions made above for a general case. In particular in the domain of initial amplitudes and times given by inequality $[\omega'_{NL}s(0)/\omega_{LN}][1-\exp(-\omega_{LN}t)]\gg 1$, the amplitude of the arrived wave packet is practically independent on its initial amplitude (its growth saturates) $s(t)\simeq(\omega_{LN}/\omega'_{NL})[\exp(\omega_{LN}t)-1]^{-1}$. In this domain the normalized amplitude of the wave-packet scales inverse proportionally to initial amplitude $[\propto 1/s(0)]$. In Fig. 6(c) this scaling law is approximately valid only for the wave packets arriving around 1.3 and 1.6 ms. In particular, the general tendency of the normalized signal to fall is obvious from the comparison of the signals 11 and 19 in Fig. 6(c). However, the changes with increasing pump amplitude in the head of the coda-type signal [around 0.7 ms$<t<$1.2 ms in Fig. 6(c)] and for the packet around 1.4 ms do not follow our simplest qualitative model. This discrepancy indicates that the processes of bulk nonlinear attenuation are not the only nonlinear processes involved. In particular, the paths of the wave packets propagation could be modified with increasing signal amplitude.

We have estimated that, in addition to hysteretic absorption through stick-slip motion of the contact between the beads [35,36], the excitation by sound of the thermal waves combined with the elastic nonlinearity of Hertzian contacts could also lead to nonlinear absorption in our experiments. The characteristic frequency f_T of relaxational absorption of acoustic energy by a contact (due to irreversible processes of heat conduction induced by inhomogeneous strain distribution in the vicinity of a contact [36]) can be estimated by equating the thermal wavelength $\lambda_T(\omega)=\sqrt{2D_T/\omega}$, where D_T is the thermal diffusivity of a material composing the beads, to the contact radius a, which provides a scale for the characteristic dimension of the importantly deformed volume [37]. This results in $f_T=\omega_T/(2\pi)=D_T/(\pi a^2)$. The radius of Hertzian contacts depends on the bead diameter D and the macroscopic strain ε through the relation $a\propto\sqrt{\varepsilon}D/2$. Thus the estimate for the frequency where the maximum acoustic decrement related to thermoelastic energy dissipation takes place is $f_T\propto(D_T/D^2)\varepsilon^{-1}$. For the values of $D_T\simeq 10^{-7}-10^{-6}$ m^2/s, $\varepsilon\simeq(3-7)\times 10^{-4}$, and $D=2$ mm in our experiments, we estimate 40 Hz$\leq f_T\leq$1 kHz. Thus for the considered sufficiently large range of parameters, the relaxational peak is importantly lower in frequency than the acoustic frequency of the wave packets launched in the medium ($f_T\ll f$). In the presence of acoustic loading with amplitude smaller than the static loading, the dimensions of the contact diminish due to acoustic field rectification caused by the nonlinearity of the Hertzian contact [37]. This forces the relaxation frequency to increase. The relaxational peak moves closer to the excitation frequency, resulting in an additional induced (nonlinear) absorption of sound [37].

A temperature rise due to the dissipation of the acoustic power into heat could have an effect on the acoustic attenuation in the medium. It is also a good candidate to explain the slow recovery of the elastic properties of the medium (or the recovery of the coda shape) at the end of the EAS by average cooling of the contacts in the medium with time. Theoretical estimates of acoustically induced temperature rise in our experimental configuration as well as temperature measurements inside the medium have been performed. The heat capacity of the granular medium, neglecting the contribution of the saturating air, can be estimated as ρC_p, where $C_p\simeq 0.75\times 10^{-3}$ J K^{-1} m^{-3} is the heat capacity per unit mass of glass and $\rho\simeq 1.4\times 10^3$ kg m^{-3} is the density of the granular medium. Considering that most of the acoustic energy is absorbed in a region of volume $V_{abs}\simeq 3\times 10^{-4}$ m^3 surrounding the emitter, the heat capacity of the region where the acoustic waves are absorbed is $C_{abs}\simeq\rho C_p V_{abs}\simeq 3\times 10^{-4}$ J K^{-1}. With the maximum generated acoustic power $P_{ac}\simeq 2$ mW during the time $t=30$ s (corresponding to one measurement at the maximum amplitude used for the results reported in this paper), and considering that all the acoustic energy is dissipated into heat, the temperature rise is estimated as

$$\Delta T \simeq \frac{P_{ac}t}{C_{abs}} \simeq 2 \times 10^{-4} \text{ K}. \quad (6)$$

This very small estimated temperature rise of the medium is not in contradiction with the performed experiments. The achieved precision in the temperature measurements using thermocouples embedded in the granular medium was better than 0.1 K. At full acoustic power of $P_{ac} \simeq 2$ mW, no temperature change has been observed, with an acoustic excitation lasting for more than 5 min. This maximizes the very small estimated average temperature rise. The average strain corresponding to estimated temperature rise (6) in the medium, i.e., the relative modification of the bead dimensions (the radius R) due to this homogeneous heating is estimated via the thermal-expansion coefficient of glass $\alpha \simeq 7.5 \times 10^{-7}$ K as

$$\frac{\Delta R}{R} \simeq \alpha T \simeq 1.5 \times 10^{-10}. \quad (7)$$

Consequently, the very small temperature rise (smaller than the room-temperature fluctuations) and the small associated strain (much smaller than the acoustic strain), derived here considering a homogeneous heating over the absorption region, are too weak to explain the observed acoustic signal modifications. However, a precise study of the heating at the level of the contact could provide important information on the possible inhomogeneous heating of the beads and temperature rise at the level of each individual contact. Friction and thermoelasticity, two possible mechanisms of acoustic energy conversion into heat, both take place at the level of the contact where most of the strain is localized. As a consequence, the heat is first generated in a volume, around the contact regions, smaller than the one considered above for homogeneous heating of the medium by a factor going from 10^4 to 10^5. In this case, the temperature rise could be locally much higher than the one estimated above and could contribute to the observed modification of the acoustic coda with amplitude.

Elastic memory effects at the level of the contacts themselves (stick-slip motion for Hertz-Mindlin contacts for instance [35]) or at the mesoscopic scale [38] could also contribute. In order to explain the slow-dynamic effects observed above the excitation strain ε_{30}, it is possible to consider that the medium state is pushed by the acoustic wave action in an out of equilibrium configuration. The distribution of the hysteretic mechanical elements (the hysteretic contacts) in the so-called Preisach-Mayergoyz plane [39–41] is modified by the wave action. The slow healing process, which could correspond to a recovering of the initial distribution of hysteretic elements of the Preisach-Mayergoyz plane, could occur through the action of thermal phonons. This process has been described in [39] in the frame of the Preisach-Arrhenius model of hysteresis.

It should be also mentioned that acoustic spectrum broadening due to generation of combination frequencies (generation of sum frequencies [17], difference frequencies [7], or subharmonics [16,18]) is accompanied by energy losses at the fundamental frequency, i.e., by the nonlinear attenuation. This is one more of the possible physical mechanisms of nonlinear absorption in our experiments.

Finally, an interesting question is the dependence of the wave-packet scattering on the packet amplitude. If we accept the simplest hypothesis that scattering is due to fluctuations of the size of the contacts along the packet propagation path, and the weaker the contact relative to average loaded contacts the stronger it scatters, then softening of the Hertzian contacts in the periodic acoustic strain field of an amplitude lower than the average strain should cause the increase in scattering, i.e., the nonlinear attenuation.

Although all the above proposed scenarios seem to be in favor of the nonlinear attenuation of sound waves and can help to understand our experimental observations, at least partially, the physical reality is obviously richer. The interesting physics in wave-packet propagation could come from the fact that the continuous distribution of contact preloading implies the existence of weakly loaded contacts (with preloading lower than the strain in the acoustic field) that could be forced clapping (to open and to close) by the wave packet. There are also noncontacting grains that could be forced to contact by the acoustic wave packet, introducing tapping (closing and opening) contacts in the medium. It could be demonstrated that under some conditions these intermittent contacts can become larger in surface area and stiffer (in average over the wave period) with increasing wave amplitude. For example, the rigidity of a clapping contact starts to grow when the acoustic strain exceeds the strain necessary for the opening of this contact (i.e., the preloading strain) about 1.5 times (see Fig. 6 in [37]). Consequently contacts of this type could, above some critical amplitude of the acoustic field, induce through the mechanisms of thermoelastic relaxational wave absorption and wave scattering, not the nonlinear acoustic attenuation but the nonlinear acoustic transparency. Thus the nonlinear phenomena in the unconsolidated granular packing under consideration here could be expected to be strongly dependent on the distribution of contact preloading.

B. Dependence of signal energy on excitation amplitude

In order to analyze these amplitude-dependent effects on the signal energy attenuation, it is adequate now to focus on the energetical properties of the signals. In Fig. 8(d), the EAS is recalled. The total energies of the high-pass filtered signals $C_{n,n}^{\mathrm{HF}}(0)$ are normalized by a quantity proportional to the excitation energy ε_n^2 both for the low excitation amplitudes of the EAS [Fig. 8(a)] and for the higher excitation amplitudes [Fig. 8(b)]. The parts comprised between the dashed lines compare the same range of normalized energy, from normalized values of 0.8–1.1 roughly, which are the extreme values taken by the signals excited with the weak probe amplitude. The lowest value observed in Fig. 8(a) corresponds to an excitation amplitude range where the parameter $R_{n,1}$ begins to decrease from one to a lower value. It is important to note that, for the normalized energies associated with the higher excitation amplitudes, in Fig. 8(b), all the values are below the region delimited by the dashed lines,

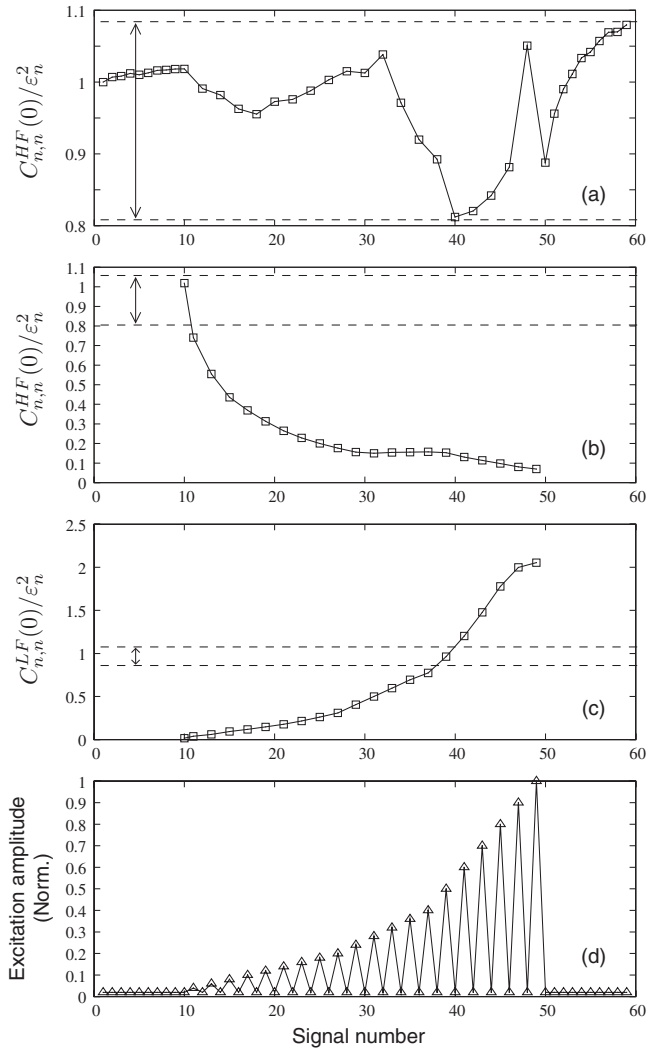

FIG. 8. (a) Energy of the high-pass filtered signals $C^{\mathrm{HF}}_{n,n}(0)$ normalized by a quantity proportional to the excitation energy ε_n^2 for the low excitation amplitudes of the EAS (d). (b) Energy of the high-pass filtered signals for the higher excitation amplitudes of the EAS (d). (c) Energy of the low-pass filtered signals for the higher excitation amplitudes of the EAS (d). (d) Excitation amplitude sequence (EAS) used in the experiment.

which means that energy absorption is always stronger for $\varepsilon_a > \varepsilon_1$ even when the acoustic response of the medium has been modified by a strong wave action (even signals $s_{40}-s_{50}$ for instance). The general behavior of the normalized energy for increasing excitation amplitudes is decreasing and monotonous: the higher the excitation amplitude is, the higher the energy absorption is. Its associated energy is consequently deviating from the ε_n^2 law. The nonlinear energy of the LF demodulated part is increasing monotonously with the excitation amplitude. The LF energy exceeds the HF energy of the signal from the excitation amplitude ε_{41}, as seen in Fig. 8(c) when the LF energy is above the region delimited by the dashed lines.

IV. SUMMARY OF THE RESULTS

Different experimental observations have been presented and the main results can be summarized as the following:

(i) observation of the coexistence of a nonlinear self-demodulated LF wave together with a HF coda-type wave (Fig. 2),

(ii) a drastic increase in the HF coda energy with static stress, compared to the dependence of the LF wave energy (Fig. 4),

(iii) a strong shape dependence of the coda on the acoustic excitation amplitude (Figs. 5 and 6), and especially a strong nonlinear attenuation of the coda wave at the latest arrival times,

(iv) almost no variation in the acoustic properties of the medium after moderate acoustic excitations up to an excitation acoustic strain of $\varepsilon_a \sim 0.3 \times 10^{-5}$, corresponding to signal number 31 (this represents a ratio of dynamic over static deformation of $\varepsilon_a/\varepsilon_0 \simeq 5 \times 10^{-3}$),

(v) dynamic modifications of the acoustic properties (nonlinear self-action, fast dynamics) even at low excitation levels $\varepsilon_a \sim 2 \times 10^{-7}$ corresponding to signal number 11 (this represents a ratio of dynamic over static deformation of $\varepsilon_a/\varepsilon_0 \simeq 3 \times 10^{-4}$),

(vi) modification of the acoustic properties after large excitation levels (slow dynamics and conditioning effects), followed by a slow recovery.

Having in mind the ray acoustic approximation in this experiment of multiple scattering of elastic waves, the first part of the coda signals can be associated with short propagation paths while the last part of the coda signals may be associated with longer propagation paths. Note that the lengths of the long propagation paths can exceed the container size by a factor of 10, which means that reflexions on the container sides may occur. In principle, nonlinear wave attenuation should be more visible on the long propagation paths than on the short ones because the distance for the accumulation of this nonlinear process is larger [25,42]. This explains the stronger effect of nonlinear wave attenuation on the last part of coda signals, which experienced longer propagation paths. The physical nature of this nonlinear wave attenuation process remains undetermined. Nonlinear scattering of the elastic waves due to opening or closing of the weakest contacts and therefore dynamic switching of propagation paths under the wave action could explain the nonlinear attenuation. This is in agreement with the drastic dependence of the HF coda wave energy transmission on the applied static stress. Nonlinear absorption of the elastic waves at the contacts by stick-slip [35] or thermoelasticity [33] processes could also contribute. Recent numerical simulations of the acoustic propagation through unconsolidated granular packings [43,44] could provide an interesting insight in the processes involved in the experimentally observed nonlinear attenuation.

For both nonlinear wave scattering and nonlinear wave absorption, the weakest contacts are supposed to be responsible for the main contribution, especially for such small acoustic excitation strains as $\varepsilon_a \simeq 10^{-7}$. Coda signals are shown to be particularly sensitive to these weak contacts, certainly due to the fact that energy is well distributed over the entire medium, including weak contacts, after few milliseconds (coda signals have durations larger than 2 ms, which corresponds to propagation paths much larger than the emitter–receiver distance). Moreover, the wavelength, being

of the order of the bead diameter ($\lambda \sim d$), small features as small as the beads and their contacts are resolved by the acoustic wave. This is not the case for small amplitude long-wavelength propagation ($\lambda \gg d$), which is known to be less sensitive to the weak contacts in the medium and more influenced by the average properties of the medium [7,9].

The modification of the acoustic properties after the application of a strong excitation is commonly related to the effect of conditioning and slow dynamics [32,33,45,46]. This addresses the problem of the acoustic wave influence on the granular medium state and memory. Under a given threshold, the medium is apparently not modified (under excitation amplitude number 31, $\varepsilon_a \simeq 0.3 \times 10^{-5}$, which corresponds to a ratio of dynamic over static deformation of $\varepsilon_a/\varepsilon_0 \simeq 5 \times 10^{-3}$), while over some excitation amplitude, the medium exhibits memory of the past acoustic excitation. Coda signal analysis is shown to be a powerful tool in monitoring slight modifications in the acoustic response of an unconsolidated granular structure as a function of time, the resolution (including some time averaging) being of the order of the second.

V. CONCLUSIONS

In this work, experimental results on the nonlinear transport of short-wavelength (of the order of the bead diameter) acoustic waves are reported. It is shown that the amplitude dependence of the codas is strong, and contains some information on the strength of the propagation paths in the medium. An amplitude-dependent attenuation is visible on the characteristic time T_e (arrival time of half the signal energy), which diminishes with the excitation amplitude: most of the nonlinear self-action effects take place at the latest arrival times of the coda signals. This shows that the field that encountered a larger number of scattering events, or that does not follow the strongest force chains is more influenced by the effects of nonlinear dissipation (stick-slip, sliding, or thermoelastic losses) and nonlinear scattering (closing or opening of the weak contacts for instance).

Among the possible applications of such experimental results is the nondestructive testing (NDT) of granular structures with nonlinear acoustic methods, in particular with multiple scattered waves (coda signals), in contrast to the widely used and recent nonlinear methods employing coherent wave interactions [47,48]. For this purpose, it would be of interest to make use in the future of the coda wave interferometry technique [49–51].

It has been shown that the acoustic properties of the medium can be modified temporarily by a strong acoustic excitation. In the context of NDT, this work shows the range of acoustic amplitudes to use (or the time necessary to recover the initial state) in order to stay in a regime where the acoustic waves do not modify the elastic response of the medium.

ACKNOWLEDGMENTS

This work is supported by ANR project "grANuLar" Project No. NT05-3 41989. The authors would like to thank E. Brasseur, E. Egon, and P. Collas for their technical help on the experimental setup.

[1] H. Jaeger and S. Nagel, Science **255**, 1523 (1992).
[2] M. E. Cates, J. P. Wittmer, J.-P. Bouchaud, and P. Claudin, Phys. Rev. Lett. **81**, 1841 (1998).
[3] P. de Gennes, Rev. Mod. Phys. **71**, S374 (1999).
[4] P. Richard, M. Nicomedi, R. Delannay, P. Ribière, and D. Bideau, Nature Mater. **4**, 121 (2005).
[5] C.-H. Liu and S. R. Nagel, Phys. Rev. Lett. **68**, 2301 (1992).
[6] C.-H. Liu and S. R. Nagel, Phys. Rev. B **48**, 15646 (1993).
[7] V. Tournat, V. Zaitsev, V. Gusev, V. Nazarov, P. Béquin, and B. Castagnède, Phys. Rev. Lett. **92**, 085502 (2004).
[8] X. Jia, Phys. Rev. Lett. **93**, 154303 (2004).
[9] V. Zaitsev, V. Nazarov, V. Tournat, V. Gusev, and B. Castagnède, Europhys. Lett. **70**, 607 (2005).
[10] D. M. Mueth, H. M. Jaeger, and S. R. Nagel, Phys. Rev. E **57**, 3164 (1998).
[11] D. L. Blair, N. W. Mueggenburg, A. H. Marshall, H. M. Jaeger, and S. R. Nagel, Phys. Rev. E **63**, 041304 (2001).
[12] X. Jia, C. Caroli, and B. Velicky, Phys. Rev. Lett. **82**, 1863 (1999).
[13] V. Tournat, B. Castagnède, V. Gusev, and P. Béquin, C. R. Mec. **331**, 119 (2003).
[14] J. Goddard, Proc. R. Soc. London, Ser. A **430**, 105 (1990).
[15] H. A. Makse, N. Gland, D. L. Johnson, and L. Schwartz, Phys. Rev. E **70**, 061302 (2004).
[16] V. Tournat, V. Gusev, and B. Castagnède, Phys. Lett. A **326**, 340 (2004).
[17] V. Tournat, V. Gusev, V. Zaitsev, and B. Castagnède, Europhys. Lett. **66**, 798 (2004).
[18] V. Tournat, C. Inserra, and V. Gusev, Ultrasonics **48**, 492 (2008).
[19] A. Tourin, A. Derode, A. Peyre, and M. Fink, J. Acoust. Soc. Am. **108**, 503 (2000).
[20] R. Weaver, J. Acoust. Soc. Am. **71**, 1608 (1982).
[21] H. P. Schriemer, M. L. Cowan, J. H. Page, P. Sheng, Z. Liu, and D. A. Weitz, Phys. Rev. Lett. **79**, 3166 (1997).
[22] K. Aki and B. Chouet, J. Geophys. Res. **80**, 3322 (1975).
[23] R. Hennino, N. Trégourès, N. M. Shapiro, L. Margerin, M. Campillo, B. A. van Tiggelen, and R. L. Weaver, Phys. Rev. Lett. **86**, 3447 (2001).
[24] P. Westervelt, J. Acoust. Soc. Am. **35**, 535 (1963).
[25] B. Novikov, O. Rudenko, and V. Timochenko, *Nonlinear Underwater Acoustics* (ASA, New York, 1987).
[26] V. Zverev, Acoust. Phys. **45**, 611 (1999).
[27] V. Zaitsev, A. Kolpabov, and V. Nazarov, Acoust. Phys. **45**, 202 (1999).
[28] V. Zaitsev, A. Kolpabov, and V. Nazarov, Acoust. Phys. **45**, 305 (1999).
[29] C. Coste and B. Gilles, Phys. Rev. E **77**, 021302 (2008).
[30] B. Gilles and C. Coste, Phys. Rev. Lett. **90**, 174302 (2003).
[31] V. Tournat, V. E. Gusev, and B. Castagnède, Phys. Rev. E **70**,

056603 (2004).
[32] P. Johnson and A. Sutin, J. Acoust. Soc. Am. **117**, 124 (2005).
[33] V. Zaitsev, V. Gusev, and B. Castagnède, Phys. Rev. Lett. **90**, 075501 (2003).
[34] M. Bentahar, H. El Aqra, R. El Guerjouma, M. Griffa, and M. Scalerandi, Phys. Rev. B **73**, 014116 (2006).
[35] R. Mindlin and H. Deresiewicz, ASME Trans. J. Appl. Mech. **20**, 327 (1953).
[36] K. Johnson, *Contact Mechanics* (Cambridge University Press, Cambridge, 1985).
[37] L. Fillinger, V. Zaitsev, V. Gusev, and B. Castagnède, Acta. Acust. Acust. **92**, 24 (2006).
[38] C. Josserand, A. Tkachenko, D. M. Mueth, and H. M. Jaeger, Phys. Rev. Lett. **85**, 3632 (2000).
[39] V. Gusev and V. Tournat, Phys. Rev. B **72**, 054104 (2005).
[40] R. A. Guyer, K. R. McCall, and G. N. Boitnott, Phys. Rev. Lett. **74**, 3491 (1995).
[41] R. Guyer, J. tenCate, and P. Johnson, Phys. Rev. Lett. **82**, 3280 (1999).
[42] L. Zarembo and V. Krasilnikov, Sov. Phys. Usp. **13**, 778 (1971).
[43] S. Luding, Nature (London) **435**, 159 (2005).
[44] O. Mouraille and S. Luding, Ultrasonics **48**, 498 (2008).
[45] D. Holcomb, J. Geophys. Res. **86**, 6235 (1981).
[46] P. Johnson and X. Jia, Nature (London) **437**, 871 (2005).
[47] Y. Zheng, R. Maev, and I. Solodov, Can. J. Phys. **77**, 927 (1999).
[48] X. Jacob, C. Barrière, and D. Royer, Appl. Phys. Lett. **82**, 886 (2003).
[49] R. Snieder, A. Grêt, H. Douma, and J. Scales, Science **295**, 2253 (2002).
[50] O. I. Lobkis and R. L. Weaver, Phys. Rev. Lett. **90**, 254302 (2003).
[51] R. Snieder, Pure Appl. Geophys. **163**, 455 (2006).